Random Set Versus Vector Based SLAM in the Presence of High Clutter

John Mullane, Samuel Keller[†], Martin Adams[‡]

Projective Space, Singapore
[†]*Swiss Federal Institute of Technology, ETH, Zurich, Switzerland*
[‡]*University of Chile, Santiago, Chile*
jmullane@projective-space.com, [†]*kellers@ethz.ch,* [‡]*martin@ing.uchile.cl*

***Abstract*—A comparison of classical vector, and recently proposed set, based Simultaneous Localisation and Mapping (SLAM) algorithms is presented, based on tests in a marine environment. An Autonomous Surface Craft (ASC) is described, which comprises a simple kayak base and a commercially available X-band marine radar. With restrictive landmark modelling, and a lack of vehicle control input information, it is demonstrated that under a random set based framework, useful results can be obtained, despite the presence of a high rate of sea clutter, caused by the rolling and pitching of the ASC on the sea surface. This work is a step towards realising an ASC capable of performing environmental or security surveillance of a marine environment.**

***Index Terms*—Autonomous Navigation, Random Finite Set (RFS) SLAM, Marine Radar, Autonomous Surface Craft**

I. Introduction

SLAM techniques, which rely on random vectors to represent sensor measurements and landmark maps, are extremely fragile under the realistic conditions of landmark detection and association uncertainty. Stemming from the seminal developments in the tracking community [1], recent SLAM investigations suggest that a landmark map is more appropriately represented as a *set* of landmarks, requiring the tools of Random Finite Set (RFS) theory, known as Finite Set Statistics (FISST) [2], [3]. By applying FISST to the SLAM problem, it has been demonstrated that the necessity for fragile map management and data association can be eliminated. A simple FISST, known as the *Probability Hypothesis Density* (PHD) provides estimates of the number of landmarks encountered in SLAM, as well as their spatial locations, taking into account a sensor's and/or landmark detection algorithm's probabilities of detection and false alarm. This is therefore adopted in this paper, in the form, of a *Rao-Blackwellized*, (RB)-PHD-SLAM approach.

This article focusses on the navigational aspects of an Autonomous Surface Craft (ASC), which must perform SLAM in a coastal environment, adopting a commercially available marine radar, shown in Figure 1(a). Due to sea movement and currents, such a small ASC frequently undergoes relatively large angular changes in its roll, pitch, and yaw angles. This results in many clutter[1] returns from the on board sensor, due to frequent impingement of the transmitted radio waves and the sea surface. In the presence of such high levels of *sea clutter*, it will be demonstrated that FISST based SLAM is the natural choice for autonomous marine applications. For comparison purposes however, it is desirable to test the FISST based SLAM performance with state of the art vector based SLAM techniques from the robotics literature. It will be demonstrated that Nearest Neighbour (NN) based data association, together with extended Kalman Filter (EKF) based SLAM (referred to as NN-EKF-SLAM) with standard map management techniques, diverges almost immediately with such high clutter levels, due to many landmark miss-associations. Therefore, for the purposes of comparison, radar detections are smoothed, thresholded and finally clustered to yield a much reduced landmark set. This of course results in a loss of information, as valid landmarks will inevitably be accidently removed in such techniques. However, this manageable, reduced size landmark set allows an NN-EKF-SLAM implementation, for comparison purposes.

[1]returned sensor readings incorrectly thought to correspond to useful landmarks.

II. Related Work

This paper is an extension of [4], which provided an initial implementation of RFS SLAM in a marine environment, without comparisons to vector based approaches.

While marine based SLAM investigations have taken place over the past few years, they have largely focussed on the underwater domain. In [5], a delayed-state SLAM approach was presented and implemented on an underwater vehicle with vision sensors. A motion estimation and map building algorithm based on the fusion of vision and sector scan sonar data was presented in [6]. SLAM implementations in a swimming pool using a line-feature approach and scanning sonar were presented in [7]. The study was extended to a semi-structured underwater scenario in [8].

In the grounded autonomous robotics community, radar sensors have been adopted by quite a number of research groups worldwide. [9] used a W-band radar sensor for feature based SLAM experimental analyses, while reflectivity patterns from leisure craft were examined in [10]. Further SLAM and mapping investigations using W-band radar were presented in [11], [12] examining the signal statistics and their influence on the resulting localisation and map estimates.

III. The ASC and the Coastal Environment

The ASC is a robotic sea-kayak which is a low cost, high load bearing platform, being highly maneuverable and capable of operating in shallow waters. It was originally developed at the Dept. of Mechanical and Ocean Engineering, MIT for experiments in autonomous navigation in rivers and coastal environments [13]. For stabilisation in the choppy waters common to the test site, lateral buoyancy aids were added to the platform, as depicted in Figure 1(a). The vehicle could be remote operated via a radio link, through the control of an on board, steerable electric thruster. A marine, X-Band radar was mounted on a 1.5m length pole above the sea surface. The X-Band radar used was the M-1832 BlackBox Radar from Furuno, powered by an on board battery. The mechanically scanned beam has a width of 3.9^o in azimuth and 20^o in elevation. The large elevation beam width makes the sensor robust to the sometimes severe pitch and roll of the ASC. A GPS receiver (Crescent Hemisphere 110), as well as a KVH Industries, Inc. DSP5000 single-axis gyroscope for 3D pose (x_k, y_k, ϕ_k) measurements were also used in the experiments. An on board processing unit logged the GPS and gyro data at a rate of 1Hz, with the radar data being sampled and logged at a scan rate of 0.5Hz - i.e. 1 full 360^o sweep of the environment required 2 seconds. Given that the distance traversed by the ASC over a single radar scan is negligible compared to its maximum range capability of 36 nautical miles, and compared to its low resolution (7.5m), the issues of distortion with mechanically scanned sensors [7] were considered insignificant in this work.

Figure 1 shows the coastal environment and the type of landmarks to be detected and used in the sea based SLAM experiments. While the unusually low mounting height of the

(a) The coastal environment and landmarks.

(b) A buoy fixed landmark.

Fig. 1: *The ASC and a typical landmark used for coastal SLAM.*

marine radar undoubtedly increases the sea clutter interference in the logged data, by adopting suitable processing algorithms, the signal can be readily used for recursive localisation and map estimation filters as demonstrated later in Section VI. For the trials carried out in this work, the radar range bin resolution, $\delta r(q)$, was set to 7.5m, with a maximum range[2] of 7.68 km.

The following section describes the extraction of landmarks from this data for the purpose of performing SLAM.

IV. Marine Radar Landmark Extraction

Noise in the radar A-Scopes[3] in coastal environments largely consists of sea clutter. Prior to performing landmark selection, the data is first classified into landmark, $\mathcal{H}_1$ hypothesis, and, in this paper, the no landmark or clutter $\mathcal{H}_0$ hypothesis, via a CFAR detector. Such probabilistic detection methods are based on an underlying assumption on the noise amplitude statistics.

1) Adaptive Coastal Landmark Detection - OS-CFAR: If S^{lin} is the linearised received radar signal amplitude[4] with any range compensation removed then the empirical sea clutter amplitude, $p(S^{\text{lin}}|\mathcal{H}_0)$ can be obtained empirically by Monte Carlo (MC) analysis over a large number of sample scans, using manually selected windows containing only radar returns from the sea. The results of such an MC analysis are shown in Figure 2 (left), together with its best fit, continuous exponential distribution,

$$p(S^{\text{lin}}|\mathcal{H}_0) = \begin{cases} \dfrac{1}{\mu_c}\exp^{-S^{\text{lin}}/\mu_c} & \text{if } S^{\text{lin}} > 0 \\ 0 & \text{Otherwise} \end{cases} \quad (1)$$

where μ_c is the clutter exponential distribution parameter. In practice, the moment μ_c may change depending on the sea state or roll / pitch of the ASC. Due to the closely lying point landmarks and to minimise potential landmark masking issues [15], an Ordered Statistics (OS)-CFAR detection method is applied to locally estimate the moment, μ_c, in each range bin, q, and derive an adaptive threshold value, $S^{\text{OS-CFAR}}(q)$.

Figure 2 (centre) shows a sample A-Scope, recorded at a particular radar bearing angle, comprising sea clutter as well as both point surface craft and extended land landmarks. The theoretical probability of false alarm $P_{fa}^{\text{OS-CFAR}}$ of the OS-CFAR processor is

$$P_{fa}^{\text{OS-CFAR}} = k_{os}\binom{2W}{k_{os}}\frac{(k_{os}-1)!(\gamma+2W-k_{os})!}{(\gamma+2W)!}, \quad (2)$$

where W is the CFAR window width either side of the particular range bin, usually referred to as the cell under test (CUT), k_{os} is the OS-CFAR k-factor and γ represents the scaling constant which determines the decision threshold to achieve a fixed rate of false alarm. The value of γ can be obtained by non-linear, numerical zero finding routines from Equation 2 according to the desired $P_{fa}^{\text{OS-CFAR}}$. A landmark is

[2]At a radar height of just over 1.5m above sea level, landmarks of height greater than 3m above sea level (ships etc) will only fall into the line of sight of the radar at distances up to approximately 10km anyway, due to the curvature of the earth. This neglects atmospheric refractional effects, which can actually increase the line of sight of a radar [14].

[3]"A-Scope" is the term used to describe the received power as a function of range, when displayed graphically as in Figure 2 (Centre).

[4]Note that for processing purposes, the linearised received power is used, however, due to the large dynamic range of the received power, a logarithmic scale is used for graphical purposes.

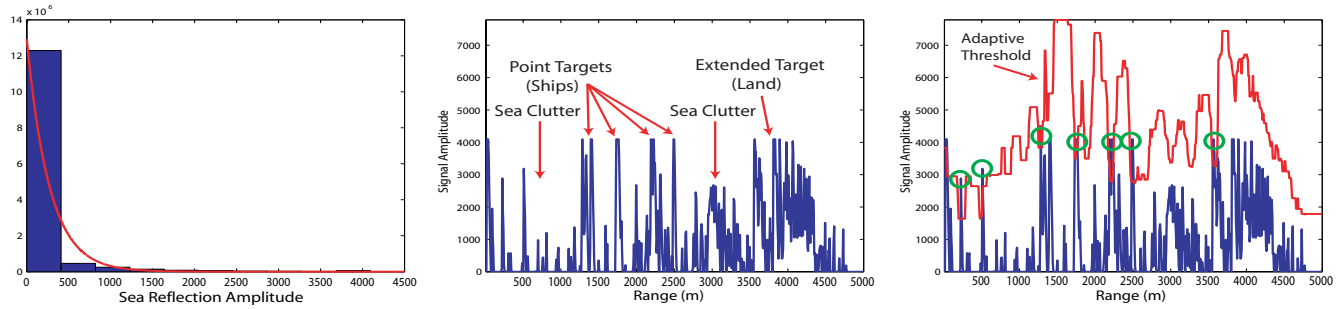

Fig. 2: *Left: The empirical sea-clutter amplitude distribution. Centre: A sample radar power vs. range spectrum showing sea clutter, point and extended landmarks. Right: An adaptive OS-CFAR detection threshold.*

considered detected in range bin q if the received power $S^{\text{lin}}(q)$ obeys

$$S^{\text{lin}}(q) \geq S^{\text{OS-CFAR}}(q) = \gamma T(S^{\text{lin}}(q)) \tag{3}$$

where $T(S^{\text{lin}}(q))$ is the test statistic determined from the cells neighbouring the CUT q according to the OS-CFAR criterion. This criterion is that the test statistic $T(S^{\text{lin}}(q))$ is chosen as the ranked power value $S^{\text{lin}}_{k_{os}}$, and that k_{os} is normally chosen to be $3W/2$ [15]. Importantly, each received power value is accompanied by a probability of detection $P_D^{\text{OS-CFAR}}$ given by

$$P_D^{\text{OS-CFAR}}(q) = \prod_{i=0}^{k_{os}-1} \frac{2W-i}{2W-i+(\gamma/2W(1+\eta^{\text{SNP}}(q)))} \tag{4}$$

where

$$\eta^{\text{SNP}}(q) = \frac{S^{\text{lin}}(q)}{S^{\text{lin}}_{k_{os}}} \tag{5}$$

The resulting threshold across all the range bins for the sample A-Scope is shown in the right hand graph of Figure 2, using the parameters, $W = 20$, $P_{fa}^{\text{OS-CFAR}} = 0.05$ and $k_{os} = (3W/2) = 30$. As can be seen, the point landmarks are detected, while most of the land reflections are suppressed. This is because land reflections have the appearance of clutter measurements. This is useful for SLAM applications, since extended landmarks are more difficult to reliably parameterise as stable landmarks. The resulting map however then reflects only point-like objects.

A 360^o *Plan Position Indicator* (PPI) scan of the coastal environment showing the power values which have exceeded the OS-CFAR threshold, is shown in Figure 3. All received power values $S^{\text{lin}}(q) < S^{\text{OS-CFAR}}(q)$ have been removed from the scan as assumed noise or sea clutter. Each of the remaining power values $S^{\text{lin}}(q) \geq S^{\text{OS-CFAR}}(q)$ were considered as valid point landmarks in the RB-PHD-SLAM experiments, each accompanied by a unique $P_D^{\text{OS-CFAR}}$. For the NN-EKF-SLAM experiment, this landmark set, which still contains many false alarms, had to be further reduced, based on image smoothing techniques.

2) Image Based Smoothing - Gaussian Filtering: Based on the point landmark detections from the OS-CFAR threshold, the regions of the measurement data are further examined to assess their likelihood of representing stable landmarks. The received power data was first converted from its natural polar

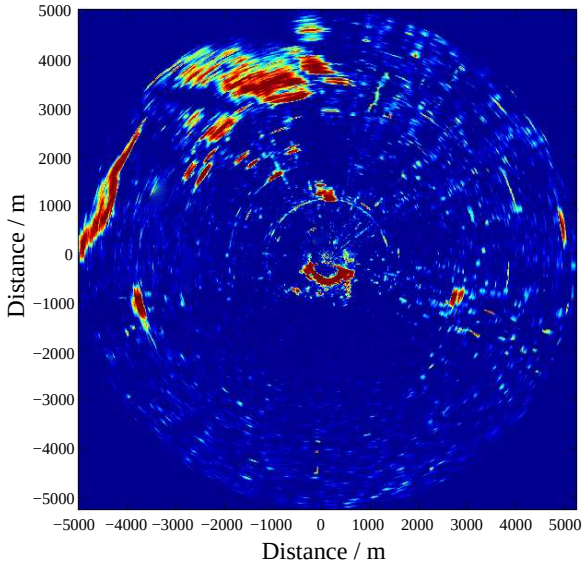

Fig. 3: *PPI display showing power values which have exceeded the $S^{\text{OS-CFAR}}$. This is the input data for the RB-PHD-SLAM experiments.*

form to Cartesian form using a weighted 4 point transformation technique, to minimise the effects of pixelation at larger ranges [16]. This form of the scan constitutes a Cartesian grid (image) with power values $S^{\log}(x, y)$, represented as colour values.

In the measurement data, landmarks rarely occupy a single range bin. Therefore, to suppress the high frequency signal fluctuations, which have successfully passed through the OS-CFAR detector, a Gaussian filter was applied to the raw data. The 2D Gaussian low pass filter [17] was convolved with the regions of the scan identified as landmarks by the OS-CFAR threshold.

3) Image Based Thresholding: To further reduce noise in the image, a simple threshold was applied and all values below the threshold were set to zero. The value was selected based on a histogram of the Gaussian smoothed radar measurements over the whole sequence. A suitable threshold for $S^{\text{lin}}(x, y)$ was then selected below which, most of the returns were assumed to still constitute noise or sea clutter.

4) Image Based Clustering: Clustering is the term used to identify parts of the radar image which belong to the same landmark. This is achieved by combining all connected pixels

which have non-zero value into one cluster. Figure 4 shows the result of clustering the thresholded image. Different colours are

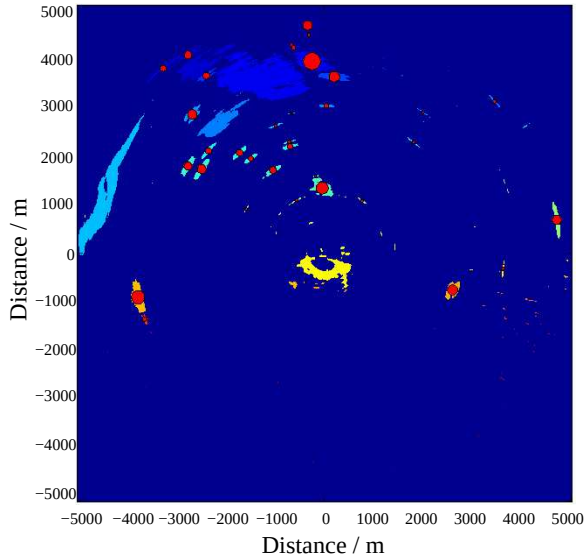

Fig. 4: *Clustering and landmark estimation, based on a thresholded, Gaussian smoothed PPI scan. This is the input data for the NN-EKF-SLAM experiments.*

used to identify different clusters.

5) Landmark Labelling: Two characteristics of each cluster are extracted in this step. First the position of the centre of area in Cartesian coordinates are determined and second the area of the cluster is determined in terms of pixel number, and converted to square meters.

The large clusters which represent parts of islands or the mainland were not used in the SLAM experiments. This is because the radar can only detect their outline partially, which leads to unreliable landmarks of changing size and position. Also a minimum size for clusters determined to be landmarks can be set, to remove some of the smaller noisy power values.

In Figure 4, the extracted landmarks are processed as described above and superimposed on to the cluster-image. The areas of the red circles correspond to the area of each cluster, and their centres are located at the centres of area of each cluster. In this example, clusters smaller than 200 m^2 and larger than 20000 m^2, as well as all landmarks within a radius of 300 meters of the radar, were deleted.

6) Comments on Landmark Reduction Techniques: Clearly with such image processing based techniques, there are many parameters which can be set to achieve a set of clusters. While the OS-CFAR detector is based on a principled $P_{fa}^{\text{OS-CFAR}}$ value, clear violations of the CFAR assumptions cause many more false alarms than those statistically expected. The image smoothing methods high-lighted here are therefore implemented as a simple means to reduce the number of false alarms. In the SLAM results, it will be shown that state of the art, vector based methods are unable to yield consistent estimates without such techniques being applied a-priori. The presented RFS based SLAM estimator will however be shown to be capable of operating on the results of the OS-CFAR processor (Figure 3) directly, without the need to resort to such ad-hoc clutter/noise reduction techniques.

V. The Marine Based SLAM Algorithms

This section describes the landmark-based SLAM algorithm implemented and analysed in this paper.

7) The ASC Process Model: Unlike ground based vehicles which are generally restricted to forward facing motion dynamics, a sea-based ASC is subject to numerous uncertain disturbances such as currents and wind, moving the ASC in any arbitrary direction. To account for these differences the following non-linear process model is adopted

$$\begin{aligned} x_k &= x_{k-1} + V_{k-1}\Delta T_k \cos(\phi_{k-1} + \delta\phi_{k-1}) + v_{k-1}^x \\ y_k &= y_{k-1} + V_{k-1}\Delta T_k \sin(\phi_{k-1} + \delta\phi_{k-1}) + v_{k-1}^y \\ \phi_k &= \phi_{k-1} + \delta\phi_{k-1} + v_{k-1}^\phi \end{aligned} \tag{6}$$

where x_k, y_k and ϕ_k represent the Easting, Northing and ASC heading angle with respect to north at time k. This can be expressed in vector form using the vehicle's state vector $X_k = [x_k \;\; y_k \;\; \phi_k]^T$:

$$X_k = F_v(X_{k-1}, U_{k-1}) + v_{k-1} \tag{7}$$

where $F_v()$ corresponds to a vehicle motion vector function encapsulating the three Equations 6 and U_{k-1} represents a vector comprising the input velocity signal and the measured angular change - i.e. $U_{k-1} = [V_{k-1} \;\; \delta\phi_{k-1}]^T$, recorded by an on board single axis gyroscope[5]. v_{k-1}^x, v_{k-1}^y and v_{k-1}^ϕ represent random perturbations in the ASC motion due to external sea forces and are modelled by white Gaussian signals, encapsulated in the noise vector $v_{k-1} = [v_{k-1}^x \;\; v_{k-1}^y \;\; v_{k-1}^\phi]^T$. $\Delta T_k = t_k - t_{k-1}$ is determined from the measurement rate of the gyro. In this experiment, for simplicity, $V_k = V_{k-1}$ and is chosen a priori due to the lack of suitable Doppler Velocity Log (DVL) sensors. This vehicle process model will be used in all of the SLAM algorithms, developed for comparison purposes, in this paper.

A. RFS SLAM with the PHD Filter

1) The RFS Measurement Model: The primary exteroceptive measurement sensor is the X-band radar. Such a sensor is prone to missed detections, false alarms, measurement noise and data association uncertainty. To encapsulate such sources of uncertainty, the RFS measurement model is adopted

$$\mathcal{Z}_k = \bigcup_{m \in \mathcal{M}_k} \mathcal{D}_k(m, X_k) \cup \mathcal{C}_k(X_k) \tag{8}$$

which incorporates the set based landmark detections $\mathcal{D}_k(m, X_k)$ and the spurious measurements $\mathcal{C}_k(X_k)$. Landmarks within the set map $\mathcal{M}_k$ are referred to as m. The individual landmark detections $z_k^i = [r_k^i \;\; \theta_k^i]^T$ comprise

[5]Note that although the gyroscopic measurements are recorded at time k, they are used to provide an estimate of the desired input change in heading at time $k-1$. Hence the input value corresponding to the gyro information is $\delta\phi_{k-1}$.

relative range and bearing measurements from the ASC pose at time k, given by

$$r_k^i = \sqrt{(x_k^i - x_k^{\text{radar}})^2 + (y_k^i - y_k^{\text{radar}})^2} + w_k^r \quad (9)$$

$$\theta_k^i = \arctan\left[\frac{y_k^i - y_k^{\text{radar}}}{x_k^i - x_k^{\text{radar}}}\right] - \phi_{k-1|k-1} + w_k^\theta \quad (10)$$

where (x_k^i, y_k^i) are the Cartesian coordinates of the ith landmark, $(x_k^{\text{radar}}, y_k^{\text{radar}})$ represents the coordinates of the radar location on the ASC and w_k^r and w_k^θ represent the radar range and bearing noise at time k respectively [9].

2) The PHD SLAM Filter: In a similar vein as the Fast-SLAM concept, the RFS-SLAM joint posterior can be factorised when the map is represented as a conditional PDF, conditioned on an entire vehicle trajectory $X_{0:k}$ - i.e.

$$p_k(X_{0:k}, \mathcal{M}_k|\mathcal{Z}_{0:k}, U_{0:k-1}, X_0) = p_k(X_{0:k}|\mathcal{Z}_{0:k}, U_{0:k-1}, X_0)p_k(\mathcal{M}_k|\mathcal{Z}_{0:k}, X_{0:k}) \quad (11)$$

where a Rao-Blackwellized implementation implies the mapping recursion is approximated by a Gaussian Mixture (GM)-PHD Filter, and the trajectory recursion by a Particle Filter [2]. $\mathcal{Z}_{0:k}$ represents the set of all measurements from time 0 to k, $U_{0:k-1}$ represents all inputs from time 0 to $k-1$ and X_0 is the initial pose of the ASC. The calculation of the particle weighting likelihood however, requires the evaluation of

$$g_k(\mathcal{Z}_k|\mathcal{Z}_{0:k-1}, X_{0:k}) = \int p(\mathcal{Z}_k, \mathcal{M}_k|\mathcal{Z}_{0:k-1}, X_{0:k})\delta M_k, \quad (12)$$

which involves a set integral over all possible maps. Note that this likelihood is simply the normalising constant of the Bayes recursion for propagating the RFS map density, $p_k(\mathcal{M}_k|\mathcal{Z}_{0:k}, X_{0:k})$ in Equation 11. The weighting likelihood can then be written,

$$g_k(\mathcal{Z}_k|\mathcal{Z}_{0:k-1}, X_{0:k}) = \frac{g_k(\mathcal{Z}_k|\mathcal{M}_k, X_k)p_{k|k-1}(\mathcal{M}_k|X_{0:k})}{p_k(\mathcal{M}_k|X_{0:k})}. \quad (13)$$

By approximating the predicted and updated RFS map densities as Poisson RFSs and setting the dummy variable $\mathcal{M}_k = \{m^{\text{chosen}}\}$, where m^{chosen} is a single landmark chosen according to a given strategy, the weighting likelihood can be determined in closed form, as a function of the probability of detection of the chosen landmark $P_D^{\text{OS-CFAR}}(m^{\text{chosen}}|X_k)$, and the updated and predicted PHDs of the map.

The map is estimated with a GM implementation of the PHD predictor,

$$v_{k|k-1}(m|X_{0:k}) = v_{k-1}(m|X_{0:k-1}) + b(m|X_k) \quad (14)$$

where $b(m|X_k)$ is the PHD of the new landmark RFS, $\mathcal{B}(X_k)$, and corrector,

$$v_k(m|X_{0:k}) = v_{k|k-1}(m|X_{0:k})\left[1 - P_D^{\text{OS-CFAR}}(m|X_k) + \sum_{z\in\mathcal{Z}_k} \frac{\Lambda(m|X_k)}{c_k(z|X_k) + \int_{\xi\in\mathcal{M}_k}\Lambda(\xi|X_k)v_{k|k-1}(\xi|X_{0:k})d\xi}\right] \quad (15)$$

where $\Lambda(m|X_k) = P_D^{\text{OS-CFAR}}(m|X_k)g_k(z|m, X_k)$ and,

$P_D^{\text{OS-CFAR}}(m|X_k)$ = the probability of detecting a landmark at m, from ASC pose X_k.

$c_k(z|X_k)$ = PHD of the clutter RFS $\mathcal{C}_k$ in Equation 8 at time k.

In contrast to vector based SLAM algorithms, the PHD map representation allows for a natural ability to average feature maps. Map estimates from N independent trajectory particles can be averaged into an expected map, even with map estimates of different size and without having to resolve the intra-map feature associations. Consequently both the expected vehicle trajectory and feature map can be determined as follows:

Given the posterior set of weights $\eta_k^{(i)}$ and particles $X_{0:k}^{(i)}$ and corresponding map PHDs $v_k^{(i)}(m|X_{0:k}^{(i)})$,

$$\left\{\eta_k^{(i)}, X_{0:k}^{(i)}, v_k^{(i)}(m|X_{0:k}^{(i)})\right\}_{i=1}^N, \quad (16)$$

and defining $\bar{\eta} = \sum_{i=1}^N \eta_k^{(i)}$ then,

$$\widehat{X}_{0:k} = \frac{1}{\bar{\eta}}\sum_{i=1}^N \eta_k^{(i)} X_{0:k}^{(i)}. \quad (17)$$

The posterior PHD of the map is then the expectation of the trajectory-conditioned PHDs and thus

$$v_k(m|X_{0:k}) = \frac{1}{\bar{\eta}}\sum_{i=1}^N \eta_k^{(i)} v_k^{(i)}(m|X_{0:k}^{(i)}). \quad (18)$$

If $\hat{\mathfrak{m}}_k = \int v_k(m|X_{0:k})dm$, is the mass of the posterior map PHD, the expected map estimate can then be extracted by choosing the $\hat{\mathfrak{m}}_k$ highest local maxima.

Further implementation details of this algorithm, including pseudo-code examples, are given in [2], [3].

B. NN-EKF-SLAM Implementation

For comparison purposes, an NN-EKF-SLAM implementation was carried out, based on the landmarks extracted in Section IV-5. As noted, NN-EKF-SLAM could only be implemented on this greatly reduced landmark set, since the numerous landmarks extracted by the OS-CFAR processor of Section IV-1, contained too many clutter measurements, causing immediate EKF filter divergence.

In contrast to RFS-SLAM, where the state to be estimated consists of a vector representation of the vehicle's trajectory $X_{0:k}$ and a set representation of the map $\mathcal{M}_k$, vector based SLAM methods proceed to estimate a single, *joint vector* state $\zeta_k = [X_k \ M_k]^T$ and hence provide an estimate of

$$p_{k|k}(\zeta_k|Z_{0:k}, U_{0:k-1}, X_0). \quad (19)$$

Landmark association, based on the Nearest Neighbour Standard Filter, was then carried out [18].

VI. Comparisons of SLAM Concepts at Sea

The ASC was remote controlled to execute a curved trajectory of over 1.8km, logging over 650 consecutive radar scans at a rate of 0.5Hz in a trial run lasting over 20 minutes. Multiple loops were traversed. The analysis focusses first on the location estimation errors from the RB-PHD-SLAM and NN-EKF-SLAM filters, followed by qualitative examinations of the estimated maps. In this set of experiments, the ground truth locations of all of the actual sea vessels in the area was not available and therefore the maps could only be examined in a qualitative manner, based on the known configuration of sea vessels and the nearby island's coastline. For the RB-PHD-SLAM filter, MC analysis is presented based on 50 sample runs using 100 trajectory particles in each trial.

1) Positional Estimation Analysis: The ground truth ASC position estimates, based on the GPS data, are shown as the labelled trajectories in Figures 5 and 6. Note that although

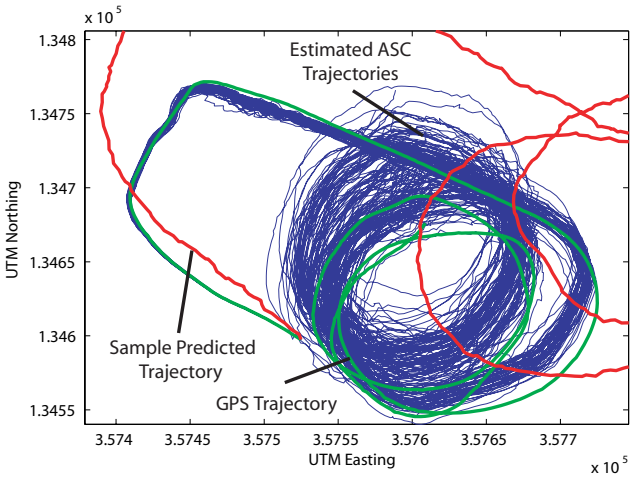

Fig. 5: *The expected trajectories from each of the 50 MC trials (blue), compared to the GPS trajectory (green).*

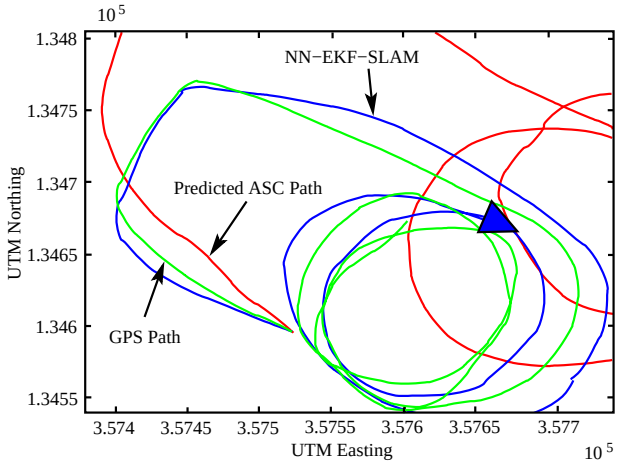

Fig. 6: *The NN-EKF-SLAM estimated path, the predicted ASC trajectory from the assumed ASC motion model and the GPS trajectory.*

GPS cannot be relied upon to provide useful, on-the-fly directional inputs, its long-term positional information is useful at reconstructing ground truth trajectory estimates.

Figure 5 depicts the estimated ASC trajectories from each of the MC runs in comparison with the GPS estimated path. A sample trajectory (red) from the assumed ASC motion model, using the measured gyroscope data, is also provided. The results demonstrate that the RB-PHD-SLAM approach yields trajectory estimates, which accurately reconstruct the traversed path, despite the sensing and vehicle modelling difficulties.

Figure 6 shows the estimated NN-EKF-SLAM path (labelled) in comparison with the GPS and predicted, motion model based trajectories. In particular, maximum displacement errors of approximately 45m, over the 1.8km trajectory, were noted for each algorithm. It should be remembered however, that NN-EKF-SLAM was only possible due to the heavily restricted landmark set necessary for reliable data association.

2) Map Estimation Analysis: Without ground truth heading information, the quality of the resulting map estimate can be used to gauge the quality of the estimated ASC heading. Since most of the point landmarks, and all of the extended landmarks (land masses), are stationary, the quality of the posterior map estimate from the temporal fusion of the measurement data provides an indication of the quality of the pose estimates. Using a linear function which relates signal power to Log-Odds occupancy [12], the posterior occupancy grid can be propagated as each X-band radar measurement arrives. A zoomed view of the posterior map estimates from the estimated trajectory is provided in Figure 7. The fused map from the RB-

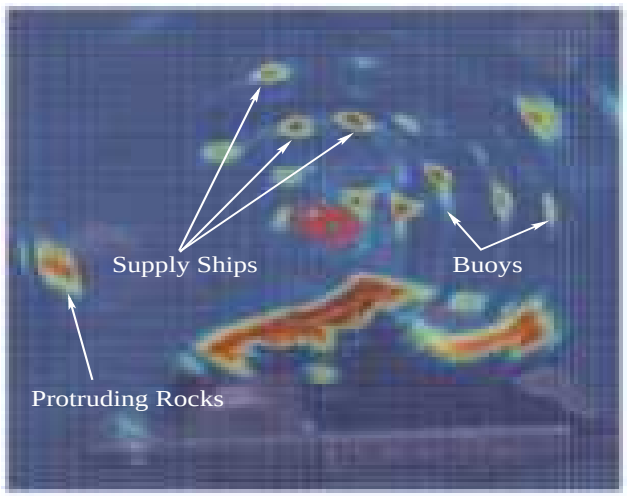

Fig. 7: *The estimated map from the RB-PHD-SLAM algorithm, in comparison to satellite imagery. The map be seen to coincide well with the islands present as well as various sea surface objects.*

PHD-SLAM estimate can be seen to match ground truth with the island coastline and various surface objects clearly evident. Some of the successfully mapped objects, identified during the experiments, are labelled in Figure 7.

To provide a comparison between the SLAM estimates from the RFS based PHD filter and the vector based NN-

EKF approach, Figure 8 shows the results of NN-EKF-SLAM during the same trial. Figure 8 shows the estimated NN-EKF-SLAM state superimposed on a satellite image of the area. The map landmarks shown are the final estimates at the end of the run. The landmarks in the vicinity of the islands (lower part of the figure) have large covariance values and are likely to result from clutter measurements, as they are sporadically introduced and deleted by the map management algorithms. Most of the mapped landmarks in the upper part of the figure correspond well with those shown in the extracted grid map of Figure 7. All of the labelled landmarks, marked as supply ships, buoys and protruding rocks, were independently identified during the experiments and correspond to those labelled in the RB-PHD-SLAM results of Figure 7.

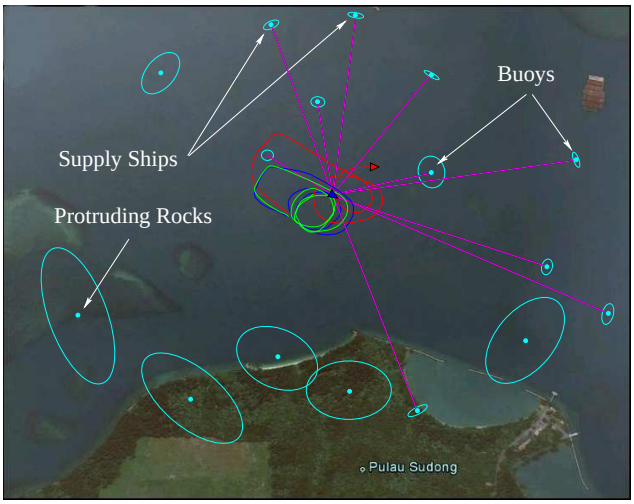

Fig. 8: *NN-EKF-SLAM results, superimposed on a satellite image of the area. The points correspond to estimated landmark locations and their corresponding ellipsi correspond to the landmarks' "3σ" uncertainty regions, magnified by a factor of 10. The lines emanating from the ASC correspond to the associated landmarks from the final estimated ASC's location. As in Figure 6, the GPS (green), estimated (blue) and predicted (red) ASC trajectories are shown.*

VII. Summary

This paper examined the possibility of SLAM using an ASC in a marine environment. Adopting an X-band radar as the main exteroceptive sensor, the investigation demonstrated that despite the widespread presence of GPS information at sea, the heading measurements can still be prone to large error. In the experiments, relative heading information was therefore provided by an inexpensive single axis, digital gyroscope.

Based on an automatic OS-CFAR point landmark detector, an RFS landmark based SLAM algorithm was developed for the ASC. The point landmarks exploited were anchored supply ships and buoys. The algorithm demonstrated how useful results are realisable, even with difficult to model vehicle dynamics and a lack of any input control measurements. Comparisons of the estimated maps demonstrate the merits of SLAM for an ASC, given uncertain heading and exteroceptive sensor measurement information. Comparative experiments were carried out with the state of the art SLAM methods NN-EKF-SLAM. To be able to successfully execute NN-EKF-SLAM, the OS-CFAR radar detections needed to be post-processed using image processing techniques, to greatly reduce the landmark set, in an attempt to reduce clutter measurements to a minimum. Only then could any qualitative comparison of NN-EKF-SLAM and the RB-PHD-SLAM filter take place.

Future work in marine environments should incorporate the extended landmarks, and should examine the possibilities of joint mapping and landmark tracking from an ASC.

Acknowledgements

This research is funded in part by the Singapore National Research Foundation through the Singapore-MIT Alliance for Research and Technology CENSAM. The authors wish to thank Akshay Rao, Anthony Yeo, Franz Hover and Nicholas Patrikalakis for their help during the sea trials.

References

[1] B.N. Vo and W.K. Ma. The Gaussian mixture probability hypothesis density filter. *IEEE Transactions on Signal Processing*, 54(11):4091–4104, November 2006.

[2] J. Mullane, B.N. Vo, M.D. Adams, and B.T. Vo. A random-finite-set approach to Bayesian SLAM. *IEEE Transactions on Robotics*, 27(2):268–282, April 2011.

[3] J. Mullane, B.-N. Vo, M. Adams, and B.-T. Vo. *Random Finite Sets for Robot Mapping and SLAM*. Springer Tracts in Advanced Robotics 72. Springer, Berlin Heidelberg, 2011.

[4] J. Mullane, S. Keller, A. Rao, M. Adams, A. Yeo, F. Hover, and N. Patrikalakis. X-band radar based SLAM in Singapore's off-shore environment. In *11th Int'l Conf. on Control, Automation, Robotics and Vision (ICARCV 2010)*, Singapore, December 2010.

[5] R.M. Eustice, H. Singh, and J.J. Leonard. Exactly sparse delayed-state filters for view-based slam. *IEEE Transactions on Robotics*, 22(6):1100–1114, December 2006.

[6] B. Kalyan, A. Balasuriya, H. Kondo, T. Maki, and T. Ura. Motion estimation and mapping by autonomous underwater vehicles in sea environments. In *Proceedings of IEEE Oceans*, pages 436–441, 2005.

[7] D. Ribas, P. Ridao, J. Niera, and J.D. Tardos. Slam using an imaging sonar for partially structured underwater environments. In *IEEE/RSJ Int'l Conf. on Intelligent Robots and Systems (IROS)*, October 2006.

[8] D. Ribas, P. Ridao, J.D. Tardos, and J. Niera. Underwater slam in a marina environment. In *IEEE/RSJ International Conference on Intelligent Robots and Systems (IROS)*, San Diego, CA, October 2007.

[9] M.W.M.G. Dissanayake, P. Newman, S. Clark, H.F. Durrant-Whyte, and M. Csorba. A solution to the simultaneous localization and map building (SLAM) problem. *IEEE Trans. Robotics and Automation*, 17(3):229–241, June 2001.

[10] G. Brooker, C. Lobsey, and R. Hennessy. Low cost measurement of small boat rcs at 94GHz. In *Proceedings of IEEE International Conference on Control, Automation and Robotics*, 2006.

[11] J. Mullane, M. Adams, and W.S. Wijesoma. Robotic mapping using measurement likelihood filtering. *International Journal of Robotics Research*, 2(28):172–190, 2009.

[12] A. Foessel, J. Bares, and W.R.L. Whittaker. Three-Dimensional Map Building with MMW RADAR. In *Proceedings of the 3rd International Conference on Field and Service Robotics*, Helsinki, Finland, June 2001.

[13] J.E. Manley. Unmanned surface vehicles, 15 years of development. In *OCEANS 2008*, pages 1–4, Sept. 2008.

[14] Merrill I Skolnik. *Introduction to Radar Systems*. McGraw Hill, New York, 1982.

[15] H. Rohling. Radar CFAR thresholding in clutter and multiple target situations. *IEEE Transactions on Aerospace and Electronic Systems*, 19(4):608–621, 1983.

[16] S. Keller. Integration of radar based robot exploration and SLAM. Technical report, NTU, Singapore, July 2010.

[17] B.K.P. Horn. *Robot Vision*. MIT Press, Cambridge, MA, 1986.

[18] Y. Bar-Shalom and T.E. Fortmann. *Tracking and Data Association*. Academic Press, 1988.